Effect of phase composition and microstructure on the thermal diffusivity of silicon nitride

G. ZIEGLER
Institut für Werkstoff-Forschung, DFVLR, 5000 Köln 90, W. Germany

D. P. H. HASSELMAN
Department of Materials Engineering, Virginia Polytechnic Institute and State University, Blacksburg, Va. 24061, USA

The effects of compositional and microstructural variables and processing conditions on the room temperature thermal diffusivity of hot-pressed and reaction-sintered silicon nitride were determined. The thermal diffusivity for hot-pressed silicon nitride increases with β-content. Maximum thermal diffusivity is reached at about 3 wt % MgO. The higher thermal diffusivity of the β-phase is attributed to its higher purity level and the less distorted crystal structure compared to the α-phase. In reaction-sintered nitride the thermal diffusivity is strongly influenced by the relative amount and needle-like morphology of the α-phase. Correlations of the thermal diffusivity with mechanical properties are discussed.

1. Introduction
The conduction of heat in dielectric materials depends strongly on the density and nature of structural lattice imperfections such as dislocations, vacancies, lattice vibrations and the degree of crystallinity [1–3]. Microstructural defects such as pores, grain boundaries (at low temperature) and microcracks also have a significant effect on heat conduction properties [4–6]. Impurities and alloying elements also are known to considerably inhibit the rate of heat conduction in dielectric materials [4, 7].

Because of their many advantageous properties, dielectric ceramics, such as silicon nitride and others, are candidate materials for high-temperature energy conversion devices such as the all-ceramic turbine or in the form of replacements for many metallic components in internal combustion engines. The performance and efficiency of such systems in addition to many other properties depend critically on the thermal conductivity and thermal diffusivity of the construction materials. High engine efficiency frequently requires a low thermal conductivity in order to minimize heat losses. On the other hand for good resistance to failure, due to thermal stresses, high values of the thermal conductivity and diffusivity are preferred. For the purposes of reliable engineering design and the achievement of the proper trade-offs it is essential that the values of thermal conductivity and thermal diffusivity of such dielectric ceramics and the variables which control them are well understood.

In this respect, silicon nitride is expected to be very complex. Silicon nitride in the hot-pressed form (HPSN) can exhibit different densities as well as different crystal structures. Hot-pressed silicon nitride can consist of varying amounts of the α-phase and the β-phase which are bonded together by a grain boundary phase. The amount, composition and crystallinity of the grain boundary phase are expected to play a major role in establishing the values for the heat conduction properties. Reaction-sintered silicon nitride (RSSN) can exhibit variations in density, free unreacted silicon content, different crystal structures as

well as a wide range of pore sizes and shape. The matrix of reaction-sintered silicon nitride consists mainly of the two modifications α and β which are different in grain size and grain shape. The α-matte containing very small pores is characterized by very thin whisker-shaped crystallites; the β-phase exists as equiaxed grains [8, 9]. All these microstructural variables are expected to effect heat conduction profoundly. The wide variation of reported values of the thermal conductivity and diffusivity of silicon nitrides including chemical vapour deposited (CVD)-Si_3N_4 and the sialons is well documented [10—14].

The purpose of the present study was to determine the thermal diffusivity of well-characterized hot-pressed and reaction-sintered silicon nitride in which, by systematic variations of grain size and composition of the starting powder and through careful process control, many of the pertinent compositional and microstructural parameters were, as far as possible, isolated.

2. Experimental procedure
2.1. Sample preparation
2.1.1. Hot-pressed silicon nitride
The microstructure of hot-pressed silicon nitride can be controlled by variation of phase composition and morphology of the starting powder and by the type and amount of sintering aids as well as by change of the processing parameters such as temperature, pressing time and pressure during the hot-pressing process [15—18]. In this investigation MgO was used as a sintering aid. To study the effect of crystal structure and the amount of glassy phase two sets of specimens were prepared:

Set I: Variation of the amount of β-phase at a constant level of 5 wt % MgO sintering aid. These specimens were hot-pressed at a temperature of 1973 K for various lengths of time to result in a certain percentage of β-phase.

Set II: Variation of the amount of MgO content between 1 and 10 wt % for a constant β-level of 100%. Specimens were hot-pressed at 2053 K. Hot-pressing time was changed in such a way that for each grade with different MgO content complete transformation was just achieved.

For the preparation of the above specimens a commercial Si_3N_4 powder* was used with a 0.04 fraction of β-phase and a specific surface area of

*H. C. Starck, Goslar, West-Germany.

496

$8.8 \, m^2 \, g^{-1}$. The impurity contents of the powder were (in wt %): 0.02 Al, 0.04 Ca, 0.04 Fe and 0.6 C. This powder was mixed with different amounts of MgO under isopropanol using a teflon container with agate balls. The powders were hot-pressed under vacuum at a pressure of $31 \, MN \, m^{-2}$. From the hot-pressed discs, 75 mm diameter and 6 mm height, circular (diameter 12.5 mm) or rectangular plates (5 mm by 5 mm) with a thickness of 2.1 mm were prepared. These samples were cut in such a way that the measured thermal diffusivity corresponded to heat flow parallel to the hot-pressing direction. Both sides of the plates were diamond ground.

2.1.2. Reaction-sintered silicon nitride
Three sets of specimens of reaction-sintered silicon nitride were prepared following procedures described elsewhere [9, 19, 20]. In Set I, artificial pores of different sizes were introduced by mixing the starting silicon powders with 4 vol % of an argon combustible wax of different particle sizes (0.36 μm; 63 to 90 μm; 125 to 180 μm). These mixtures were isostatically pressed and the wax particles were burnt out at 653 K. In Sets II and III, at nearly constant total porosity the pore structure was varied by using different grain sizes of the starting silicon powder (< 10 μm; 10 to 37 μm; 37 to 63 μm). These specimens were prepared by injection-moulding. The specimens of all three sets nitrided at 1673 K for 100 h in a mixture of 90 vol % N_2 and 10 vol % H_2 at a constant pressure of 950 mbar. More experimental details of the nitridation procedure are given in [9].

2.2. Microstructural and crystallographic characterization
The density was determined by the Archimedes principle using H_2O at 293 K for HPSN and mercury at 293 K and atmospheric pressure for RSSN. Pore and grain structure of HPSN and RSSN were examined by light and scanning electron microscopy on etched and unetched sections and on fracture surfaces. The contents of the α- and β-phases were established by quantitative X-ray crystallography. The free Si content was determined by means of optical metallography and by X-ray crystallography. For HPSN quantitative grain size data were determined from polished and etched surfaces (etching with $HF + H_2O_2 + HNO_3$
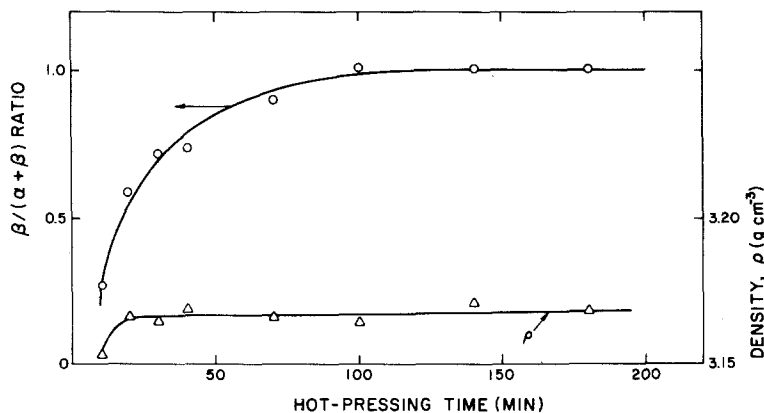
— determination of the mean grain intercept [17, 18]). For RSSN changes in the distribution of the pore-opening diameter of the bottle-shaped pores (micropores) were determined using mercury pressure porosimetry. The degree of nitridation in RSSN was calculated from the weight grain during the nitriding process [8]. The morphology of the α-phase in RSSN was determined on Ar ion-etched microsections [8] and on unetched fracture surfaces.

2.2.1. Hot-pressed silicon nitride

During the hot-pressing process at temperatures above 1773 K a liquid phase is formed and the α-crystals dissolve in the liquid and the β-crystals are precipitated. Using MgO as sintering aid the molten magnesia silicates at the grain boundaries solidify during cooling mainly in the glassy state. The thickness of the grain boundary phase is of the order of 10 to 100 Å [17]. During the α to β transformation an elongated growth of β-crystals takes place due to different growth rates perpendicular and parallel to the c-axis [17]. The mean grain size varies from 0.3 to 1.5 μm with a shortest diameter of the rod-like β-grains between 0.2 and 2 μm and the length of the elongated grains up to 10 μm.

Fig. 1 shows the density and the $\beta/\alpha+\beta$ ratio of the hot-pressed specimens of Set I with 5 wt% MgO as a function of hot-pressing time at 1973 K. The densification occurs in the early stage of the hot-pressing process. As expected, the β-content increases with increased duration at temperature. The kinetics of the α to β transformation are strongly influenced by the amount of the glassy phase, the number of the pre-existing β-grains in the starting powder and the processing conditions such as temperature and pressure during hot-

pressing [15–17]. With regard to the amount of the sintering aid this means that the time required for complete conversion of the α-Si$_3$N$_4$ to β-Si$_3$N$_4$ decreases with increasing MgO content.

Fig. 2 shows the change in microstructure during α to β transformation in Set I. After a short hot-pressing time a fine-grained mostly equiaxed grain structure is observed. With increasing hot-pressing time a change in grain morphology from equiaxed to prismatic rod-like grains takes place accompanied by the growth of elongated grains.

For the specimens in Set II, Fig. 3 gives the density as a function of MgO content for hot-pressing times required for a 100% conversion of the α- into the β-phase. The density indicates a slight decrease with increasing MgO content. The deviations from the theoretical density of 3.20 g cm^3 are probably the result of the relatively high amount of the grain boundary glassy phase. For all MgO contents the microstructure consists of elongated β-grains. The values of the mean grain intercepts are in the range 0.7 to 1.2 μm. No systematic changes in grain size were observed.

2.2.2. Reaction-sintered silicon nitride

Table I lists the data for the microstructural characterization of the RSSN samples. As indicated by Morgan [21] a number of questions on the nature of the formation of the α- and β-phase in RSSN still remain to be answered. For the method of preparation used for the specimens of this study, the α-phase is most probably formed by a gas-phase reaction between the Si and/or SiO and N$_2$, which leads to whisker-shaped crystallites in the form of a matte. At nitriding temperatures below the melting point of Si, the β-phase is formed by a diffusion process of the nitrogen to the Si–Si$_3$N$_4$ interface [8, 9]. As indicated by the
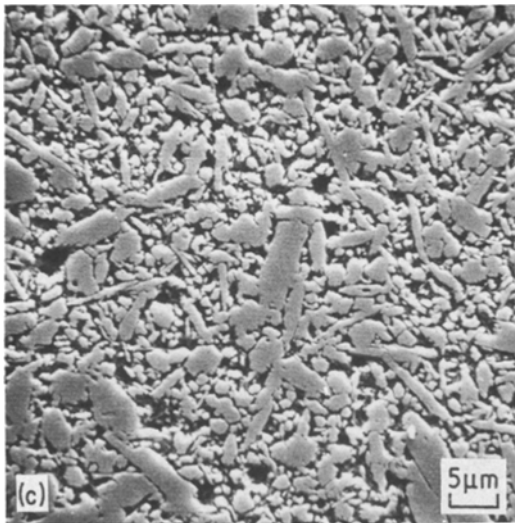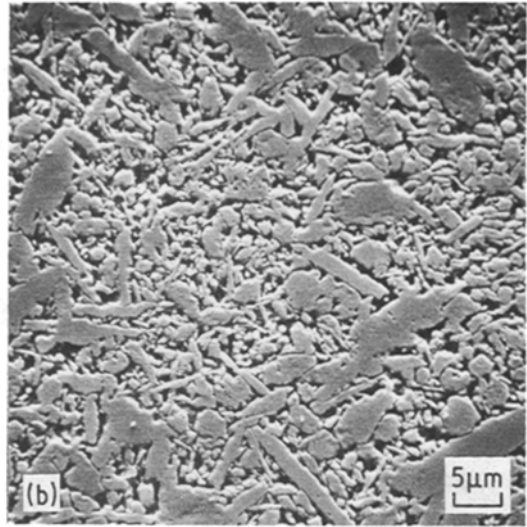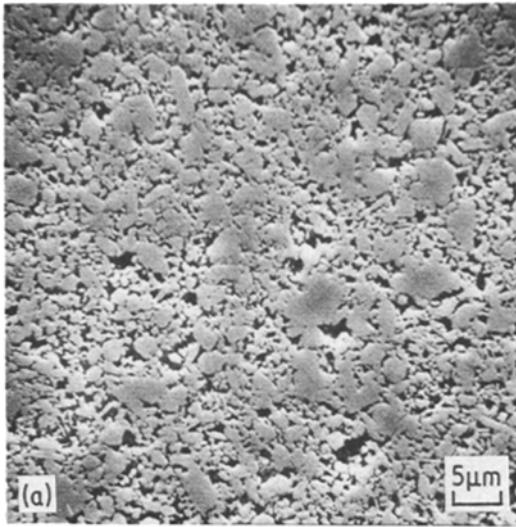
Figure 2 Change in grain morphology with increasing $\beta/\alpha+\beta$ ratio in silicon nitride with 5 wt % MgO hot-pressed at 1973 K for (a) 10 min, (b) 40 min and (c) 100 min.

data in Table I, the size of the natural pores in Sets II and III range from about 0.06 to 0.25 μm for the micropores and from 7 to 34 μm for the macropores. The micropores are thought to corre-

spond to the spacings between the very fine fibres in the α-matte [8]. The β-grains were found to be equiaxed, ranging in size from about 0.5 to 3 μm. Further microstructural details for these materials were presented in earlier publications [8, 19].

In Set I, when the other microstructural parameters are nearly constant only the size of the artificially introduced macropores is changed. In Sets II and III the amount of α-phase decreases from batches A to C, while the diameter of the micro- and macropores increases. The change in the $\alpha/\alpha+\beta$ ratio and in the size of micro- and macropores is due to the variation of the grain size of the starting silicon powder and to the corresponding change in size and arrangement of pores in the green body [9]. Fig. 4 shows the microstructures of the α-phase for the two specimens A and C of Set III, which exhibited large
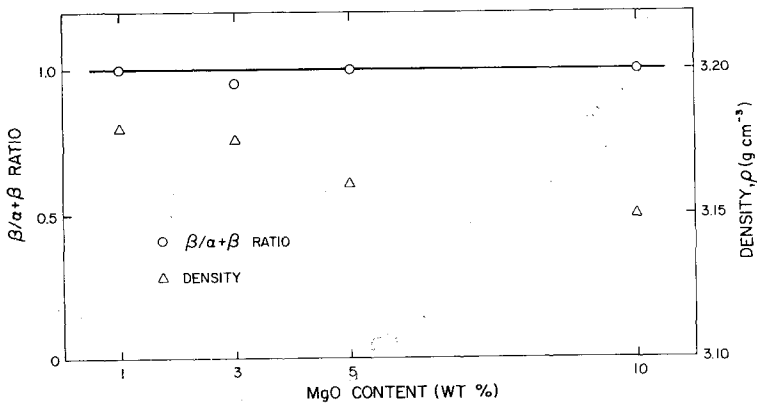

Figure 3 Density of hot-pressed silicon nitride of Set II as a function of MgO content for hot-pressing times required to result in $\beta/\alpha+\beta$ ratio equal to unity.

TABLE I Microstructural and compositional characteristics of reaction-sintered Si_3N_4

Specimen set and number	Density (g cm^{-3})	Degree of reaction (%)	$\dfrac{\alpha}{\alpha+\beta}$	Pore size (μm)		Si content (wt %)
				Micro	Macro*	
I D1	2.39	92.8	0.71	0.137	48†	1–2
I D2	2.39	92.5	0.73	0.129	66	1–2
I D3	2.41	90.1	0.64	0.097	100	1–2
II A	2.25	97.3	0.78	0.130	8	3–5
II B	2.17	96.8	0.75	0.240	22	3–5
II C	2.23	96.8	0.66	0.250	34	3–5
III A	2.41	89.9	0.82	0.058	7	1–3
III B	2.42	91.0	0.70	0.108	19	1–3
III C	2.38	93.0	0.60	0.152	28	1–3

*Mean pore size (50%) from cumulative pore size distribution.
†Arithmetic mean value of artificial pores.

differences in thermal diffusivity for the same density. These micrographs clearly indicate the difference in morphology, in particular the increase in thickness and in contact area between the fibres in batch C.

2.3. Technique for measuring the thermal diffusivity

The thermal diffusivity was measured by the laser flash technique [11]. Samples of the silicon nitride in the form of thin rectangular or circular plates were flashed on one side by means of a 50 J glass-Nd laser. A liquid N_2-cooled infra-red detector coupled to a storage oscilloscope was used to monitor and record the transient temperature as a function of time which permitted calculation of the thermal

diffusivity [22]. Measurements were made only at room temperature, at which any differences in the thermal diffusivity are expected to be most pronounced without having to resort to specimen cooling and major equipment modifications.

2.4. Elastic properties, strength and fracture toughness

Frequently for porous materials, correlation is found between the amount of pore phase, pore morphology and the thermal and mechanical properties. For this reason, experimental data for the mechanical behaviour can assist in the proper interpretation of the thermal property data. For the samples of reaction-sintered silicon nitride of the present study, the elastic properties, fracture
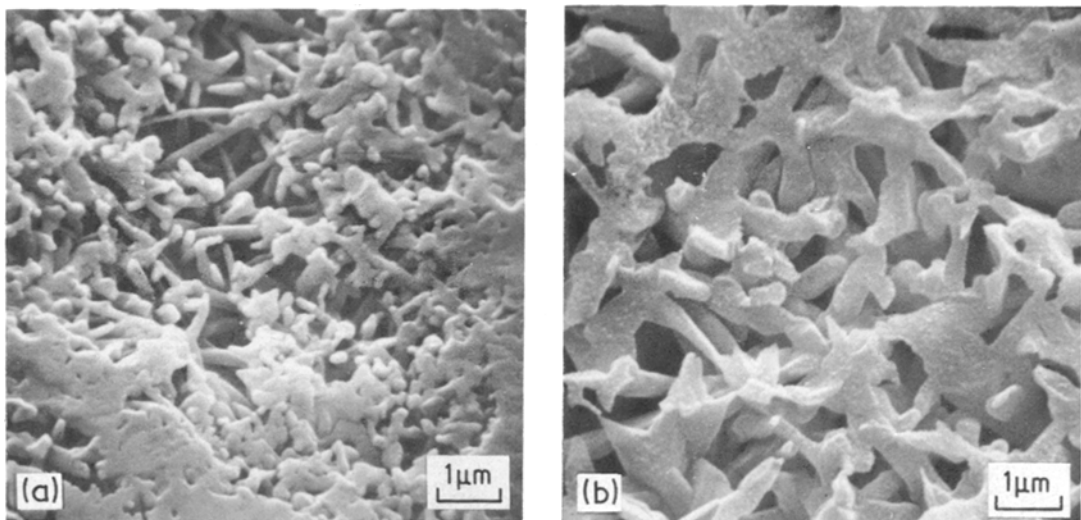

Figure 4 Microstructures of α-matte in reaction-sintered silicon nitride of Set III with large differences in room temperature thermal diffusivity (a) 0.06 cm^2 sec and (b) 0.11 cm^2 sec.

TABLE II Thermal diffusivity, tensile strength, elastic properties and fracture toughness of reaction-sintered Si_3N_4

Specimen set and number	Thermal diffusivity (cm^2 sec^{-1})	Tensile strength ($MN\,m^{-2}$)	Young's modulus ($\times 10^{-3}$ $MN\,m^{-2}$)	Poisson's ratio	Fracture toughness ($MN\,m^{-3/2}$)
I D1	0.099	140	161	0.22	1.87
I D2	0.101	119	167	0.23	1.81
I D3	0.098	101	165	0.24	1.93
II A	0.058	205	139	0.20	2.5
II B	0.083	139	127	0.23	2.08
II C	0.100	124	133	0.24	2.0
III A	0.60	150	171	0.23	2.80
III B	0.084	164	160	0.22	2.68
III C	0.109	127	154	0.24	2.14

stress (determined in 4-point bending tests) and fracture toughness were reported in detail as part of a previous study [19]. The results are shown in Table II.

3. Experimental results and discussion
3.1. Hot-pressed silicon nitride
Fig. 5 shows the thermal diffusivity of the silicon nitride with 5% MgO as a function of hot-pressing time. As indicated in Fig. 1, increasing hot-pressing time results in the transformation of the α-phase into the β-phase. Comparison of Figs 1 and 5 clearly indicates that the thermal diffusivity shows a significant increase with increasing β content.

Some explanations for this observation can be given. For very short hot-pressing times ($t_p = 10$ min) the increase can be attributed to an increase in density. For the samples subjected to longer hot-pressing times in which complete densification occurred, the increase in thermal diffusivity must be attributed to changes in the relative amounts of the α- and β-phase and to corresponding changes in grain morphology and heat transfer behaviour.

It is expected that heat conduction in the α- and β-silicon nitride at room temperature occurs primarily by phonon transport. For this reason, differences in the thermal diffusivity must arise because of differences in the phonon velocity or phonon free path. Since the elastic properties and density of α- and β-Si_3N_4 do not differ significantly (as far as the authors are aware) a difference in thermal diffusivity due to differences in phonon velocity seems unlikely. Phonon mean free path differences can be attributed to at least two possible effects. Firstly, differences appear to exist in the crystal structure of the α- and β-modifications.

Henderson and Taylor [23] suggested that the α-phase has a more strained crystal structure than the β-phase. For this reason, phonon scattering is
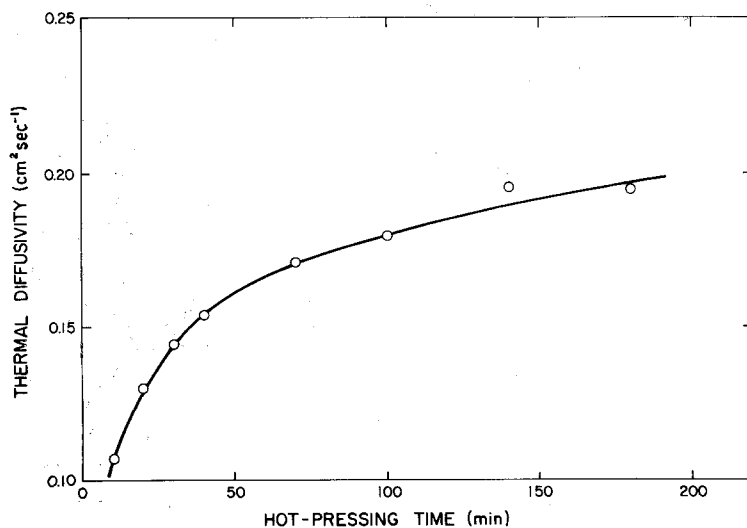

Figure 5 Thermal diffusivity at room temperature of hot-pressed silicon nitride with 5% MgO (Set I) as a function of hot-pressing time at 1973 K.
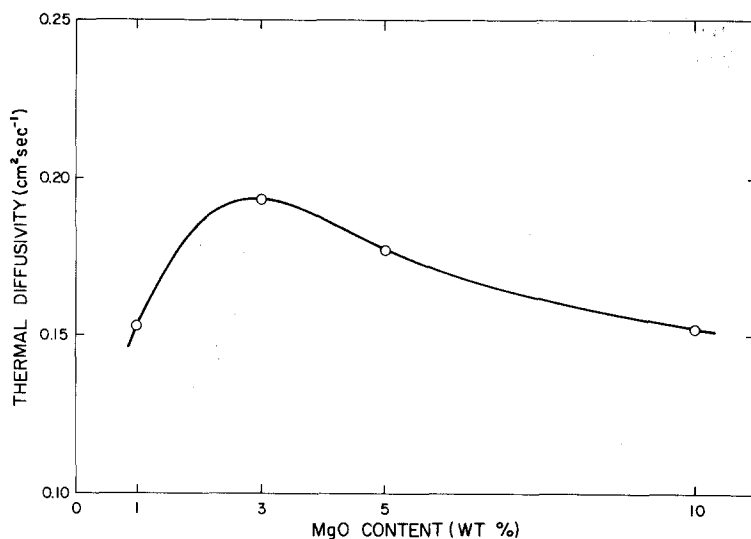
Figure 6 Thermal diffusivity at room temperature of silicon nitride hot-pressed at 2053 K (Set II) with $\beta/\alpha+\beta = 1$ as a function of MgO content.

expected to occur to a greater degree in the α-phase than in the β-phase, thereby yielding a lower value for the thermal diffusivity of the former.

A second reason for this increase in thermal diffusivity with increasing β content may be related to the formation and growth mechanism of the β-Si$_3$N$_4$. Although still a topic of discussion [24], the formation of the β-phase is thought to result from the dissolution of the α-phase in the liquid grain boundary and a reprecipitation of the silicon nitride in the β-form [17]. It is likely that the solubility of impurities in the β-phase is lower than in the liquid grain boundary phase. For this reason, it is expected that during the α to β transformation an enrichment of the impurities in the grain boundary phase occurs, so that the purity of the β-grains is higher than the original α-grains. Impurities or other atoms are well-known to be effective phonon scatterers [4, 7] so the higher purity of the β-phase is responsible for its higher diffusivity.

The differences in the size, shape and orientation of the β-grains compared to the α-grains should also be examined as possible contributing factors to the observed increase in thermal diffusivity. Since the phonon mean free path in the silicon nitride at room temperature is much smaller than the grain size any effect of the latter appears unlikely. A change in grain shape for randomly oriented grains contained in a matrix, as may be inferred from the analytical results of Bruggeman [25] and Niesel [26], should not lead to a change in thermal diffusivity. However, as shown by Powers [27] from the results of Fricke [28] an elongation of the grains in a preferred orientation will result in an increase or decrease

in the direction of heat flow parallel and perpendicular to the direction of referred orientation, respectively, regardless of the relative values of the thermal conductivities of the two phases. However, since the β-grains are elongated perpendicular to the hot-pressing direction [29, 30] and the direction of heat flow, the present observation cannot be attributed to this latter effect. Therefore, it can be concluded that the increase in thermal diffusivity with increasing β content after complete densification must be because the thermal conductivity/diffusivity of the β-phase is inherently higher than that of the α-phase.

Fig. 6 shows the data for the thermal diffusivity as a function of MgO content after complete α-to-β transformation. As can be noted, with increasing MgO content, the thermal diffusivity first increases to a maximum followed by a decrease at the highest values of MgO content. The initial increase in thermal diffusivity at low MgO content is thought to be due primarily to a reduction in residual porosity with increasing MgO content. Maximum thermal diffusivity is reached at about 3% MgO. This MgO content is commonly used in practice to achieve optimum mechanical behaviour. The decrease in thermal diffusivity with higher MgO content can most likely be attributed to the increasing amount of glassy grain boundary phase. Glassy materials generally have values of thermal conductivity or diffusivity some order of magnitudes less than crystalline solids. For high MgO contents the higher amount of magnesium silicates is expected to be particularly effective in controlling the overall rate of heat transfer through hot-pressed MgO–Si$_3$N$_4$.

3.2. Reaction-sintered silicon nitride

Table II lists the experimental data for the thermal diffusivity, elastic properties, strength and fracture toughness for all specimens of Sets I, II and III. Comparisons with the microstructural and compositional data in Table I leads to the following correlations and conclusions.

The data for the specimens of Set I, which were prepared to ascertain the effect of macropore size on thermal mechanical properties with other microstructural variables being nearly constant, showed that no such pore size effect exists for the thermal diffusivity and Young's modulus, in agreement with theory [31]. The decrease in strength with increasing macropore size is in accordance with theoretical considerations based on pore size to flaw size ratios [32, 33].

The data for the specimens of Sets II and III indicate a pronounced negative correlation between the thermal diffusivity and $\alpha/\alpha+\beta$ ratio and a positive correlation with the size of the micro- and macropores. As indicated by the data for Set I, this variation in thermal diffusivity cannot be attributed to the variation in size of the macropores. The negative correlation between the strength and the size of the macropores is to be expected from pore size to flaw size considerations, referred to earlier.

Particularly noteworthy for the data for Sets II and III is the strong negative correlation between the thermal diffusivity and the strength at nearly constant Young's modulus.

The above observations and correlations are not in general agreement with the behaviour of single-phase brittle structural materials. For these, with decreasing density, strength shows the greatest relative decrease followed by Young's modulus, thermal conductivity and thermal diffusivity in accordance with theoretical predictions [34–38]. Also, in the absence of radiation heat transfer, thermal conductivity and diffusivity should be unaffected by pore size.

An answer to these observations must be found in the unique microstructure of reaction sintered silicon nitride. Fibrous microstructures, due to the long path-length for phonon heat transfer will exhibit a much lower thermal conductivity [39] than a matrix with the same relative density containing isolated equidimensional pores. For this reason, the thermal conductivity/ diffusivity of RSSN is expected to decrease with increasing α content. Furthermore, differences

in fibre morphology for a given α content are expected to affect the thermal diffusivity as well. Generally, the smaller the thickness and inter-spacing of the fibres for constant bulk density the lower will be the thermal conductivity, in part due to increase phonon scattering at the fibre surfaces, reduced contact areas between the fibres and reduction in heat transport by the gaseous phase and radiation within the pores. For this reason, the observed variations in the thermal diffusivity for the present RSSN samples are due primarily to differences in morphology and the relative amount of α-phase. This effect is enhanced further because, as stated earlier, the lower thermal diffusivity of the α-phase compared to the β-phase is thought to be due to the more distorted crystal structure of the former.

The inverse correlation between strength and thermal diffusivity at near constant Young's modulus, particularly noticable for the specimens of Set II, probably also can be attributed to the amount and size of the α-fibres. An increase in fibre amount is expected to improve the fracture toughness, as observed, which improves strength.

The free Si content does not seem to have a pronounced effect on the thermal diffusivity, possibly because, relatively, the Si content is small.

3.3. General

It should be noted that although for both the hot-pressed and reaction-sintered silicon nitride the thermal diffusivity increases with increasing β-content, these effects occur for different reasons. For the hot-pressed silicon nitride, the more perfect crystal structure and the higher purity of the β-phase leads to an increase in the thermal diffusivity. In the reaction-sintered silicon nitride, however, the fibrous morphology and amount of the more strained α-silicon nitride appears to be the deciding factor in establishing the value of the thermal diffusivity.

The results of the present study suggest that, by careful process modifications, a measure of control can be exerted over the heat conduction properties of silicon nitride. For high thermal stress resistance which requires high thermal conductivity the relative amount of the β-phase should be maximized. For reaction-sintered silicon nitride, however, this latter approach involves an undesirable trade-off with a decreasing strength. On the other hand, for engine components which require low thermal conductivity in order to maintain high engine efficiency because of reduced heat losses, the

502

relative α content should be kept as high as possible for both the hot-pressed as well as the reaction-sintered silicon nitride.

Acknowledgments

References

1. R. BERMAN, "Thermal Conductivity in Solids" (Clarendon Press, Oxford, 1976).
2. H. J. SIEBENECK, W. P. MINNEAR, R. C. BRADT and D. P. H. HASSELMAN, *J. Amer. Ceram. Soc.* **59** (1976) 84.
3. K. CHYUNG, G. E. YOUNGBLOOD and D. P. H. HASSELMAN, *ibid.* **61** (1978) 590.
4. W. D. KINGERY, H. K. BOWEN and D. R. UHLMANN, "Introduction to Ceramics", 2nd edn. (John Wiley, New York, 1975).
5. H. J. SIEBENECK, D. P. H. HASSELMAN, J. J. CLEVELAND and R. C. BRADT, *J. Amer. Ceram. Soc.* **58** (1976) 241.
6. D. P. H. HASSELMAN, *J. Comp. Mater.* **12** (1978) 403.
7. J. E. MATTA and D. P. H. HASSELMAN, *J. Amer. Ceram. Soc.* **58** (1975) 458.
8. J. HEINRICH and G. STREB, *J. Mater. Sci.* **14** (1979) 2083.
9. J. HEINRICH, Deutsche Forschungs and Versuchsanstalt fur Luft-und Raumfahrd (DFVLR), Report number FB 79-32, DFVLR, 500 Cologne 90, FRG.
10. W. GEORGE, *Proc. Brit. Ceram. Soc.* **22** (1973) 147.
11. F. F. LANGE, H. J. SIEBENECK and D. P. H. HASSELMAN, *J. Amer. Ceram. Soc.* **59** (1976) 454.
12. T. HIRAI, S. HAYASHI and K. NIIHARA, *Amer. Ceram. Soc. Bull.* **57** (1978) 1126.
13. M. KURIYAMA, Y. INOMATA, T. KUJIMA and Y. HASEGAWA, *ibid.* **57** (1978) 1119.
14. R. J. LUMBY, B. NORTH and A. J. TAYLOR, in "Ceramics for High Performance Application — II", edited by J. J. Burke, E. N. Lenoe and R. N. Katz (Brook Hill Publishing Co., Chesnut Hill, Mass., 1978) pp. 893–906.
15. H. KNOCH and G. ZIEGLER, *Sci. Ceram.* (1977) 494.
16. *Idem, Ber. Dt. Keram. Ges.* **55** (1978) 4, 242.
17. H. KNOCH and G. E. GAZZA, *Ceramurgia International,* in press.
18. G. ZIEGLER and H. KNOCH, unpublished work.
19. G. ZIEGLER and J. HEINRICH, *Ceramurgia International*, in press.
20. J. HEINRICH, D. MUNZ and G. ZIEGLER, (in preparation).
21. P. E. D. MORGAN, *J. Mater. Sci.* **15** (1980) 791.
22. W. J. PARKER, R. J. JENKINS, C. P. BUTLER and G. L. ABOTT, *J. Appl. Phys.* **32** (1961) 1697.
23. C. M. B. HENDERSON and D. TAYLOR, *Trans. J. Brit. Ceram. Soc.* **2** (1975) 49.
24. H. M. JENNINGS, S. C. DANFORTH and M. H. RICHMAND, *J. Mater. Sci.* **14** (1979) 1013.
25. D. A. G. BRUGGEMAN, *Ann. Physik* **24** (1935) 636.
26. W. NIESEL, *ibid.* **10** (1952) 336.
27. A. E. POWERS, Conductivity in Aggregates, Knolls Atomic Power Laboratory, Pittsburgh, Pennsylvania, Report number KAPL-2145, March 1961.
28. H. FRICKE, *Phys. Rev.* **24** (1924) 575.
29. F. LANGE, *J. Amer. Ceram. Soc.* **57** (1974) 84.
30. *Idem, ibid.* **56** (1973) 518.
31. Z. HASHIN, *J. Appl. Mech.* **29** (1962) 143.
32. O. L. BOWIE, *J. Math. Phys.* **35** (1956) 60.
33. F. ERDOGAN, in "Fracture Mechanics of Ceramics", Vol. 1, edited by R. C. Bradt, D. P. H. Hasselman and F. F. Lange (Plenum Press, New York, 1974).
34. R. M. SPRIGGS, *J. Amer. Ceram. Soc.* **44** (1961) 628.
35. D. P. H. HASSELMAN, *ibid.* **45** (1962) 452.
36. L. RAYLEIGH, *Phil. Mag.* **34** (1892) 48.
37. J. C. MAXWELL, "A Treatise on Electricity and Magnetism", 3rd edn. (Oxford University Press, Oxford, 1904).
38. E. H. KERNER, *Proc. Phys. Soc. (London)* **B69** (1956) 802.
39. H. J. SIEBENECK, R. A. PENTY, D. P. H. HASSELMAN and G. E. YOUNGBLOOD, *Amer. Ceram. Soc. Bull.* **56** (1977) 572.